© 2014. Published by The Company of Biologists Ltd | Development (2014) 141, 2506-2515 doi:10.1242/dev.105551

RESEARCH ARTICLE

Cadherin 6 promotes neural crest cell detachment via F-actin regulation and influences active Rho distribution during epithelial-to-mesenchymal transition

Matthew R. Clay[1,2,3] and Mary C. Halloran[1,2,3,*]

ABSTRACT

The epithelial-to-mesenchymal transition (EMT) is a complex change in cell phenotype that is important for cell migration, morphogenesis and carcinoma metastasis. Loss of epithelial cell adhesion and tight regulation of cadherin adhesion proteins are crucial for EMT. Cells undergoing EMT often display cadherin switching, where they downregulate one cadherin and induce expression of another. However, the functions of the upregulated cadherins and their effects on cell motility are poorly understood. Neural crest cells (NCCs), which undergo EMT during development, lose N-cadherin and upregulate Cadherin 6 (Cdh6) prior to EMT. Cdh6 has been suggested to suppress EMT via cell adhesion, but also to promote EMT by mediating pro-EMT signals. Here, we determine novel roles for Cdh6 in generating cell motility during EMT. We use live imaging of NCC behavior *in vivo* to show that Cdh6 promotes detachment of apical NCC tails, an important early step of EMT. Furthermore, we show that Cdh6 affects spatiotemporal dynamics of F-actin and active Rho GTPase, and that Cdh6 is required for accumulation of F-actin in apical NCC tails during detachment. Moreover, Cdh6 knockdown alters the subcellular distribution of active Rho, which is known to promote localized actomyosin contraction that is crucial for apical NCC detachment. Together, these data suggest that Cdh6 is an important determinant of where subcellular actomyosin forces are generated during EMT. Our results also identify mechanisms by which an upregulated cadherin can generate cell motility during EMT.

KEY WORDS: Cadherin, Neural crest, RhoGTPase, Cell adhesion, EMT, zebrafish

INTRODUCTION

Epithelial-to-mesenchymal transition (EMT) is a remarkable process in which cells lose epithelial structure and undergo major changes in cell shape, adhesion and motility to become migratory. EMTs are crucial for many morphogenetic cell movements and for tissue formation during development. Moreover, aberrant activation of EMT underlies several pathologies, including carcinoma metastasis (Nieto, 2011; Thiery et al., 2009). Thus, uncovering molecular mechanisms that drive EMT is essential for understanding the development and mechanisms of cancer progression and other diseases.

The cadherin family of cell-adhesion molecules plays a central role in mediating epithelial cell adhesions via adherens junctions. The process of 'cadherin switching', where cells change expression from one cadherin to another, is a hallmark of EMT that remains poorly understood (reviewed by Wheelock, 2008). Although cadherin-based cell adhesions must be downregulated for delamination from epithelia, the purpose and function of upregulated cadherins is less clear. It has been suggested that cadherin upregulation may be important for cells undergoing EMT to segregate from other epithelial cells or to increase cell motility (Maeda et al., 2005; Wheelock et al., 2008). Cadherins can promote cell motility in a variety of cell types through mechanisms apart from their roles in adhesion (Maeda et al., 2005; McCusker et al., 2009; Nieman et al., 1999; Park and Gumbiner, 2012, 2010; Shoval et al., 2007). Furthermore, cadherins influence several signaling pathways associated with motility, such as growth factor and Rho GTPase signaling (Betson et al., 2002; Bryant et al., 2005; Doherty et al., 2000; Kashef et al., 2009; Kim et al., 2000; Kovacs et al., 2002; Noren et al., 2003; Perrais et al., 2007; Qian et al., 2004; Skaper et al., 2001); however, roles for these cadherin-signaling functions during EMT are largely unknown. In general, the molecular mechanisms downstream of cadherin switching that induce cell motility are not well understood.

Neural crest cells (NCCs) undergo EMT from the neuroepithelium during normal development and display several changes in cadherin expression, making them ideal for studying cadherin-switching functions in EMT. Because NCC derivatives can give rise to neuroblastoma and melanoma, elucidation of NCC EMT mechanisms is important for understanding the biology of these cancers. In many cell types, including some carcinoma cells, the cadherin switch associated with EMT involves decreased E-cadherin (Ecad) and increased N-cadherin (Ncad) levels (Wheelock et al., 2008). Interestingly, NCCs display a different, dynamic cadherin expression profile. In the early neural plate all cells express Ecad, which is replaced by Ncad during neurulation (Dady et al., 2012; Hatta et al., 1987). However, this Ecad-to-Ncad switch does not induce NCC EMT or ectopic EMT of other neuroepithelial cells (Dady et al., 2012). Instead, NCC EMT occurs later and is associated with reduced Ncad levels and increased Cadherin 6 (Cdh6; formerly cadherin 6B in chick) levels (Inoue et al., 1997; Nakagawa and Takeichi, 1995, 1998; Park and Gumbiner, 2010). The role of Cdh6 in EMT has remained unclear, in part because Cdh6 knockdown experiments have produced diverse results. Studies showing that Cdh6 knockdown increases NCC delamination from chick midbrain and that *cdh6* is downregulated by Snail2 support the theory that Cdh6-meditated adhesion inhibits NCC EMT (Coles et al., 2007; Taneyhill et al., 2007). In contrast, other studies showing that signaling through Cdh6 mediates de-epithelialization, loss of cell polarity and increased migratory ability in trunk NCCs suggest that Cdh6 promotes EMT (Park and Gumbiner, 2012, 2010). These differing results suggest that Cdh6 may have diverse and context-dependent functions in EMT. Because signaling pathways regulating cell motility can be highly influenced by the extracellular

[1]Cell and Molecular Biology Program, University of Wisconsin, Madison, WI 53706, USA. [2]Department of Zoology, University of Wisconsin, Madison, WI 53706, USA. [3]Department of Neuroscience, University of Wisconsin, Madison, WI 53706, USA.

*Author for correspondence (mchalloran@wisc.edu)

Received 30 October 2013; Accepted 23 April 2014

Development (2014) 141, 2506-2515 doi:10.1242/dev.105551

environment (Bergert et al., 2012; Provenzano and Keely, 2011; Sahai and Marshall, 2003; Tozluoglu et al., 2013), it is important to investigate molecular mechanisms controlling EMT in the natural cellular environment.

To date, how Cdh6 affects live cell dynamics during EMT has not been investigated, partly due to challenges in identifying and imaging premigratory NCCs during the initial cell behavior changes in the neuroepithelium. We previously imaged zebrafish NCC behaviors during EMT in the intact *in vivo* environment (Berndt et al., 2008; Clay and Halloran, 2013). An important early behavior in EMT is the actomyosin-driven detachment of the apical NCC tail, which correlates with a loss of cell junctions, is preceded by accumulation of F-actin in apical regions of the cell and requires activation of the GTPase Rho specifically in the same subcellular region (Ahlstrom and Erickson, 2009; Clay and Halloran, 2013). Cdh6 is enriched in apical regions of NCCs and can affect regulators of F-actin (Park and Gumbiner, 2012, 2010), suggesting that it could function in apical detachment. Furthermore, the presence or absence of specific cadherins can influence activation of Rho GTPases (Charrasse et al., 2007, 2002; Johnson et al., 2004; Kouklis et al., 2003; Lampugnani et al., 2002; Taniuchi et al., 2005), suggesting that cadherin switching may regulate GTPase signaling. However, few studies have examined how cadherins affect the subcellular distribution of GTPase activation, which is important for cell motility and EMT (Bravo-Cordero et al., 2013; Clay and Halloran, 2013; Heasman et al., 2010; Itoh et al., 2002; Machacek et al., 2009; Matthews et al., 2008; Nakaya et al., 2008; Nalbant et al., 2004; Pertz et al., 2006).

Here, we have used live imaging to uncover functions of Cdh6 in EMT and in the molecular mechanisms underlying this process. We imaged NCC motile behaviors, as well as the spatiotemporal dynamics of F-actin and active Rho *in vivo*. We found that Cdh6 knockdown decreased NCC EMT and specifically led to failure of NCC detachment without affecting other NCC behaviors. NCCs that fail to detach after Cdh6 knockdown rarely accumulate apical F-actin, suggesting that Cdh6 regulates this subpopulation of F-actin during EMT. Finally, we show that Cdh6 knockdown results in an expanded area of Rho activation within NCCs. Together, our data identify new roles for Cdh6 in promoting specific motile behaviors required for EMT, and reveal novel mechanisms by which Cdh6 promotes EMT.

RESULTS

Cdh6 expression and distribution are highly regulated

Cdh6 protein and mRNA are expressed in the chick dorsal neural tube and are downregulated in NCCs shortly after EMT (Coles et al., 2007; Nakagawa and Takeichi, 1998; Park and Gumbiner, 2010; Taneyhill et al., 2007). Similarly, in the developing zebrafish (*Danio rerio*) *cdh6* is expressed early in the neural keel where NCCs develop (Liu et al., 2006). However, an analysis of *cdh6* expression relative to neural crest markers at various stages of EMT has not been carried out in any system. We examined expression patterns of *cdh6* and the NCC marker *sox10* with *in situ* hybridization during early, middle and late stages of NCC EMT in zebrafish. As expected, *cdh6* was expressed in the dorsal neuroepithelium of the forebrain, hindbrain and trunk. At 14 hours post fertilization (hpf), when many NCCs begin EMT (Berndt et al., 2008; Clay and Halloran, 2013), *cdh6* was absent from the midbrain and broadly expressed in the hindbrain (Fig. 1B) in a pattern similar but not identical to *sox10* (Fig. 1E). By 16 hpf, when many NCCs are actively undergoing EMT, *cdh6* expression was slightly stronger but showed a more restricted pattern (Fig. 1C). The highest levels of *cdh6* were at the midbrain-hindbrain boundary and near rhombomere boundaries, whereas *sox10* was markedly decreased throughout the neuroepithelium (Fig. 1F). By 18 hpf, when most NCC EMT is complete, *cdh6* expression was very strong and broad throughout the hindbrain (Fig. 1D), and few if any *sox10*-expressing cells remained in the neuroepithelium (Fig. 1G). These data suggest that the timing and level of *cdh6* expression may be associated with distinct functions in NCCs and neuroepithelial cells. Because *cdh6* and *sox10* show similar expression patterns during early EMT, we examined the overlap of *cdh6* and *sox10* with fluorescent two-color *in situ* hybridization at 14 hpf. We found extensive co-expression of *cdh6* and *sox10* in premigratory NCCs (Fig. 1H, closed yellow arrowheads). However, there were cells in the hindbrain that expressed only *cdh6* (Fig. 1H, open yellow arrowheads) or only *sox10* (Fig. 1H, open white arrowheads). Outside the neuroepithelium most NCCs expressed only *sox10* (Fig. 1H, closed white arrowheads). In summary, low levels of *cdh6* are seen primarily in NCCs before and during EMT. After NCCs delaminate, *cdh6* becomes highly expressed throughout the neuroepithelium in cells that do not undergo EMT. These results show that the distribution and level of *cdh6* are tightly spatiotemporally controlled during hindbrain NCC EMT and suggest that moderate levels of *cdh6* are associated with NCC EMT.

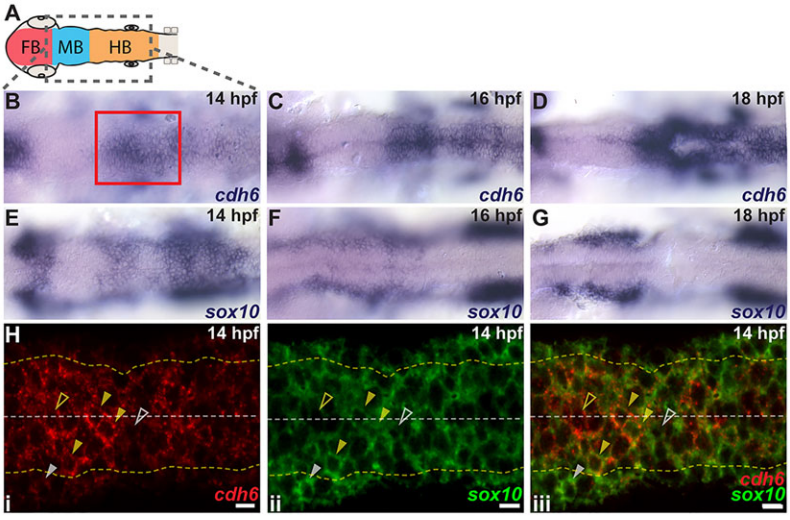

Fig. 1. *cdh6* is expressed dynamically in the hindbrain and NCCs. (A) Embryonic brain divisions. Gray box shows region displayed in B-G. (B-G) Dorsal views (anterior left) of *cdh6* and *sox10 in situ* hybridizations at 14 hpf (B,E), 16 hpf (C,F) and 18 hpf (D,G). Red box marks approximate area shown in H. (H) Confocal images (dorsal views, anterior left, individual *z*-planes) of fluorescent *in situ* hybridizations for *cdh6* (i, iii) and *sox10* (ii, iii) at 14 hpf. Yellow dashed lines mark basal neuroepithelial surfaces and white dashed lines mark apical midlines. Cells between the yellow dashed lines are neuroepithelial cells or premigratory NCCs. Cells outside the yellow dashed lines are mesenchymal cells or delaminated NCCs. Closed yellow arrowheads mark premigratory NCCs expressing *cdh6* and *sox10*. Open yellow arrowheads mark neuroepithelial cells expressing only *cdh6*. Open white arrowheads mark NCCs expressing only *sox10*. Closed white arrowheads mark NCCs outside the neuroepithelium expressing only *sox10*. FB, forebrain; MB, midbrain; HB, hindbrain. Scale bars: 10 μm.

Development (2014) 141, 2506-2515 doi:10.1242/dev.105551

To explore the distribution of Cdh6 protein, we examined Cdh6 fusion proteins in the neuroepithelium. We injected *cdh6-mCherry* mRNA, which should result in exogenous Cdh6 throughout the embryo, into one-cell stage transgenic embryos where NCCs express GFP [*Tg(-4.9sox10:EGFP)*] (Wada et al., 2005). Interestingly, at 14 hpf Cdh6-mCherry was membrane localized in many neuroepithelial cells, but appeared to be excluded from most NCCs (Fig. 2B, Table 1). However, after we knocked down endogenous Cdh6 using a splice-blocking morpholino (*cdh6*SplMO; see below) that does not target exogenous Cdh6, we saw Cdh6-mCherry in significantly more premigratory NCCs (Fig. 2C, Table 1), suggesting that the presence of endogenous Cdh6 affected the ability of NCCs to properly localize exogenous Cdh6. To test whether Cdh6 distribution was affected by Ncad, we injected Cdh6-mCherry mRNA into Ncad-morphant embryos. With Ncad knockdown, Cdh6-mCherry was observed in neuroepithelial cells; however, Cdh6-mCherry was excluded from most NCCs (Fig. 2D, Table 1), suggesting that reducing Ncad is not sufficient to allow exogenous Cdh6 expression in NCCs.

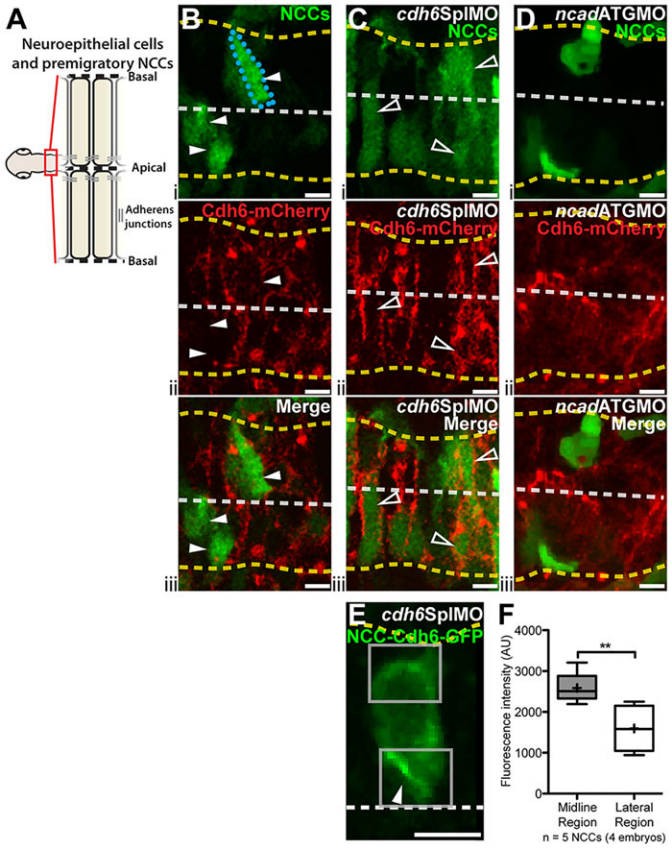

Fig. 2. Exogenous Cdh6 distribution is tightly regulated. (A) Imaging region and neuroepithelial structure. (B-E) Confocal images (dorsal views, anterior left) of living 14 hpf embryos injected with *cdh6-mCherry* mRNA (B-D) or *−4.9sox10:GFP* (E). Yellow dashed lines mark basal neuroepithelial surfaces and white dashed lines mark apical midlines. (B-D) Single confocal *z*-planes showing Cdh6-mCherry (ii, iii) in transgenic embryos with GFP-labeled NCCs (i, iii). (B) Cdh6-mCherry is rarely seen in NCCs (arrowheads and outlined NCC) after *cdh6-mCherry* mRNA injection alone. (C) More NCCs express Cdh6-mCherry (open arrowheads) after *cdh6*SplMO injection. (D) Few NCCs express Cdh6-mCherry with Ncad knockdown (*ncad*ATGMO). (E) Confocal *z*-projection of Cdh6-GFP in a premigratory NCC. Boxes show ROIs measured. (F) Cdh6-GFP intensity is elevated in midline regions relative to lateral regions of NCCs (***P*=0.0056, unpaired one-tailed *t*-test). AU, arbitrary units. Line is median, + is mean, box covers upper and lower quartiles, and bars encompass minimum and maximum values. Scale bars: 10 μm.

Table 1. Proportion of GFP-labeled NCCs expressing Cdh6-mCherry

Group	Number of hindbrain NCCs	Number of GFP+mCherry positive NCCs (%)
Tg(-4.9sox10:EGFP) +*cdh6-mCherry* mRNA	30	5 (16.7%)*
Tg(-4.9sox10:EGFP) +*cdh6-mCherry* mRNA +*cdh6*SplMO	46	21 (45.7%)*,‡
Tg(-4.9sox10:EGFP) +*cdh6-mCherry* mRNA +*ncad*ATGMO	49	11 (22.4%)‡

*P=0.013 Fisher's exact test.
‡P=0.019 Fisher's exact test.

To more precisely examine the subcellular distribution of exogenous Cdh6 in NCCs, we injected plasmid DNA to express Cdh6-GFP in NCCs (*-4.9sox10:cdh6-GFP*), along with *cdh6*SplMO. The resulting mosaic expression pattern allowed us to examine Cdh6-GFP in individually labeled premigratory NCCs, and we found Cdh6-GFP biased toward the apical midline of premigratory NCCs (Fig. 2E,F). Together, our data show that expression levels and distribution of Cdh6 are strictly regulated, likely both transcriptionally and post-transcriptionally, and that regulation of Cdh6 is independent of Ncad.

Cdh6 knockdown prevents NCC apical detachment and subsequent NCC EMT

Because Cdh6-mediated effects on live NCC behaviors had not been examined and its functions may be highly context dependent, we set out to determine whether Cdh6 controls motile cell behaviors *in vivo*. We combined Cdh6 knockdown with live imaging of NCC behavior *in vivo*. We designed a Cdh6 splice-blocking morpholino (*cdh6*SplMO) that resulted in either complete or partial deletion of the targeted exon, caused frame shifts and resulted in no detectable wild-type transcript (supplementary material Fig. S1). Injection of either the splice-blocking morpholino or a translation-blocking morpholino (*cdh6*ATGMO; Kubota et al., 2007) decreased levels of Cdh6 protein (supplementary material Fig. S1F). For live imaging, we injected morpholinos along with plasmid DNA to express membrane-bound GFP mosaically in NCCs (*−4.9sox10:GFP-CAAX*) and live-imaged behaviors of individual cells during the entire EMT process. In embryos injected with scrambled control morpholino (*control*MO), NCCs exhibited stereotypical behaviors during delamination from the neuroepithelium (Fig. 3A,B; supplementary material Movie 1). In contrast, knockdown of Cdh6 with either morpholino specifically inhibited apical detachment of premigratory NCCs (Fig. 3C,D; supplementary material Movie 2), which is one of the first observable motile behaviors of NCC EMT (Ahlstrom and Erickson, 2009; Clay and Halloran, 2013). We previously reported that 71.2% of NCCs analyzed with this method underwent apical detachment and completed EMT during imaging in *control*MO-injected embryos (Clay and Halloran, 2013). We found significantly fewer NCCs completing EMT following Cdh6 knockdown (*cdh6*SplMO=41.6%, n=24 NCCs in five embryos, P=0.032 Fisher's exact test; *cdh6*ATGMO=31.6%, n=19 NCCs in three embryos, P=0.0094 Fisher's exact test). Of NCCs that failed to undergo EMT, 77.8% remained in contact with the apical midline at the end of imaging (n=27 NCCs in eight embryos injected with either morpholino), indicating that disruption of EMT is typically due to failure of apical detachment. NCCs that failed to detach exhibited another characteristic NCC behavior: blebbing at the basal side of the cell

Development (2014) 141, 2506-2515 doi:10.1242/dev.105551

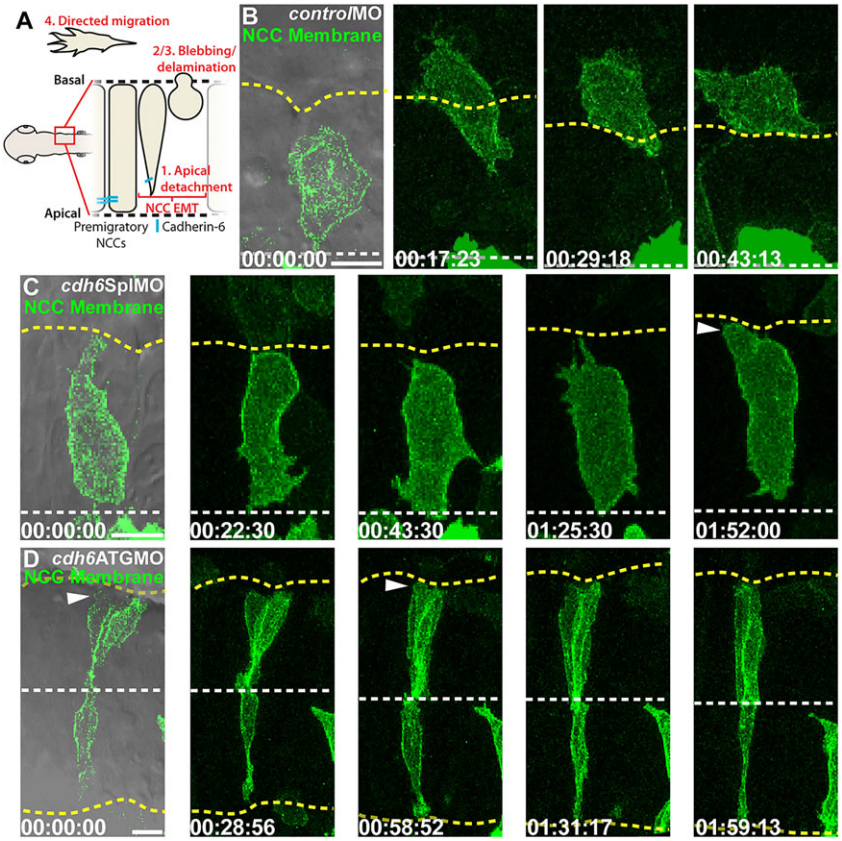

Fig. 3. Cdh6 knockdown reduces NCC detachment and EMT. (A) NCC EMT behaviors and imaging region. (B-D) Time-lapse images (dorsal views, anterior left, confocal *z*-projections, beginning at 14 hpf) of NCCs expressing GFP-CAAX. First frames show a single DIC plane for reference. Yellow dashed lines mark basal neuroepithelial surfaces and white dashed lines mark apical midlines. (B) Control morpholino (*control*MO) injection does not affect NCC behaviors or EMT. (C,D) Cdh6 knockdown with *cdh6*SplMO (B) or *cdh6*ATGMO (C) disrupts apical detachment and EMT. However, NCCs do exhibit blebbing (arrowheads). Time=h:min:s. Scale bars: 10 μm.

(Fig. 3C,D; arrowheads, supplementary material Movie 2). This suggests that Cdh6 does not regulate blebbing, and that blebbing alone is not sufficient to generate motility within the neuroepithelium. Importantly, NCCs showed similar behaviors after injection of either morpholino, and the decrease in EMT did not differ between morpholinos (P=0.7554 Fisher's exact test), suggesting that the effects were specific to Cdh6 knockdown.

To test whether Cdh6 function in EMT is NCC-autonomous, we generated mosaic embryos via blastula stage cell transplantations (Fig. 4A). In donor embryos, all cells were labeled with Texas Red-dextran and NCCs also expressed GFP [Tg*(-4.9sox10:EGFP)*]. Host embryos were injected with Cdh6 morpholinos. Donor cells were transplanted at 3 hpf and host embryos were imaged at 14 hpf. Donor NCCs were identified as having both green and red fluorescence. We examined only donor NCCs in areas where the neuroepithelium contained no other donor-derived wild-type cells (n=12 NCCs in four embryos). Of these, 10 NCCs (83.3%) underwent EMT. Four of the 10 cells delaminated from the neuroepithelium and initiated migration during imaging, whereas the remaining six cells were in the position of newly delaminated NCCs at imaging onset and migrated away from the neuroepithelium. Fig. 4C shows one example of an individual donor NCC undergoing the full process of EMT. These data show that individual NCCs with normal Cdh6 levels can undergo EMT when surrounded by Cdh6-knockdown cells, indicating that the functions of Cdh6 in detachment and EMT are NCC-autonomous.

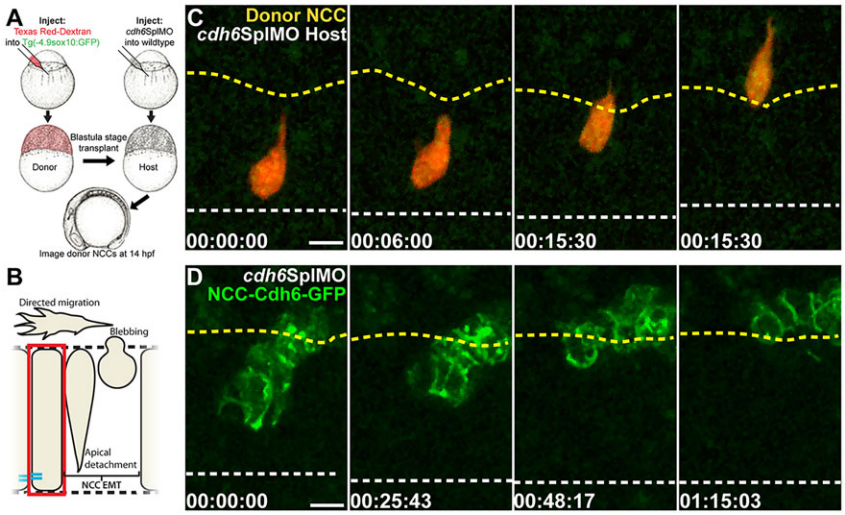

Fig. 4. Cdh6 function in EMT is NCC autonomous and Cdh6-GFP rescues morpholino knockdown. (A) Cell transplantation experiments. (B) Imaging region in C,D. (C,D) Confocal *z*-projections (dorsal views, anterior left) showing NCCs that were in the neuroepithelium at imaging onset. Time-lapse imaging began at 14 hpf. Yellow dashed lines mark basal neuroepithelial surfaces and white dashed lines mark apical midlines. (C) A wild-type donor NCC (red/green) undergoes EMT normally when transplanted into a Cdh6 knockdown embryo. (D) NCCs expressing Cdh6-GFP undergo EMT as a cluster in Cdh6 knockdown embryo. Time=h:min:s. Scale bars: 10 μm.

Development (2014) 141, 2506-2515 doi:10.1242/dev.105551

To further test morpholino specificity, we tested whether Cdh6-GFP expressed in NCCs (*−4.9sox10:cdh6-GFP*) could rescue EMT in Cdh6 morphant embryos. During time-lapse imaging, all premigratory NCCs in the neuroepithelium that expressed Cdh6-GFP underwent EMT (n=11 NCCs in two embryos). These results indicate that the defect in NCC detachment is specific to loss of Cdh6. Interestingly, we began imaging at a stage when many NCCs should still be initiating EMT (14 hpf). However, at this stage the majority of NCCs expressing Cdh6-GFP were already located outside the neuroepithelium (72.4%, n=127 NCCs in 24 embryos). This result suggests the level of Cdh6-GFP driven by the *sox10* promoter may be high enough to induce early EMT. Furthermore, cells expressing Cdh6-GFP often appeared to delaminate collectively (Fig. 4D), suggesting high levels of Cdh6-GFP may also cause ectopic cell clustering. This clustering was not seen in transplant experiments, where donor cell Cdh6 levels were not manipulated. Together, these results identify a specific, NCC-autonomous role for Cdh6 in generating NCC motility, by promoting apical NCC detachment and EMT.

To ask whether Cdh6 regulates NCC detachment indirectly by affecting Ncad, we tested whether Cdh6-mCherry affects the distribution of Ncad. Cdh6 knockdown had no effect on the distribution of Ncad-GFP (supplementary material Fig. S2A,B). Moreover, Cdh6-mCherry expression could not rescue neuroepithelial defects resulting from Ncad knockdown (data not shown) or mutation (supplementary material Fig. S2C,D), suggesting these cadherins do not have equivalent functions. These data indicate that Cdh6 promotes EMT via a mechanism that does not involve indirect modulation of Ncad.

Cdh6 is important for apical F-actin accumulation during NCC detachment

We previously showed that F-actin accumulates in apical NCC tails prior to actomyosin-driven detachment (Clay and Halloran, 2013). However, it remained unknown what signals are important for establishing this specific F-actin distribution. Cdh6 affects signaling of the F-actin regulators LIM kinase 1 (LIMK1) and cofilin, and is enriched in apical regions of chick NCCs (Park and Gumbiner, 2012, 2010), similar to the pattern we observed with Cdh6-GFP (Fig. 2E,F). This suggests it could regulate apical F-actin. We tested this hypothesis by imaging a biosensor for F-actin (mCherry-UtrCH; Burkel et al., 2007) that we had used previously (Berndt et al., 2008; Clay and Halloran, 2013). We injected plasmids to label NCCs with membrane-bound GFP (*−4.9sox10:GFP-CAAX*) and the F-actin biosensor (*−4.9sox10:mCherry-UtrCH*), and imaged EMT behaviors. In controls, the majority of labeled cells underwent EMT (n=12/15 NCCs in three embryos) and F-actin accumulated in apical tails prior to detachment (Fig. 5B, white arrowheads; supplementary material Movie 3). We quantified F-actin levels in the apical tail by normalizing against F-actin in blebs (see Materials and Methods). We found that, in the tail, F-actin levels spiked prior to detachment (Fig. 5C), and that accumulations of F-actin were relatively stable (lifetime ≥0.5 min; Table 2). In Cdh6-knockdown embryos, the majority of NCCs failed EMT (10/12 NCCs in three embryos), and F-actin accumulation was rarely observed in the apical tail (Fig. 5D, closed yellow arrowheads; supplementary material Movie 4). Quantification showed that F-actin levels did not increase in NCCs that did not detach (Fig. 5E), and F-actin accumulations were less stable in these cells (Table 2). However, in

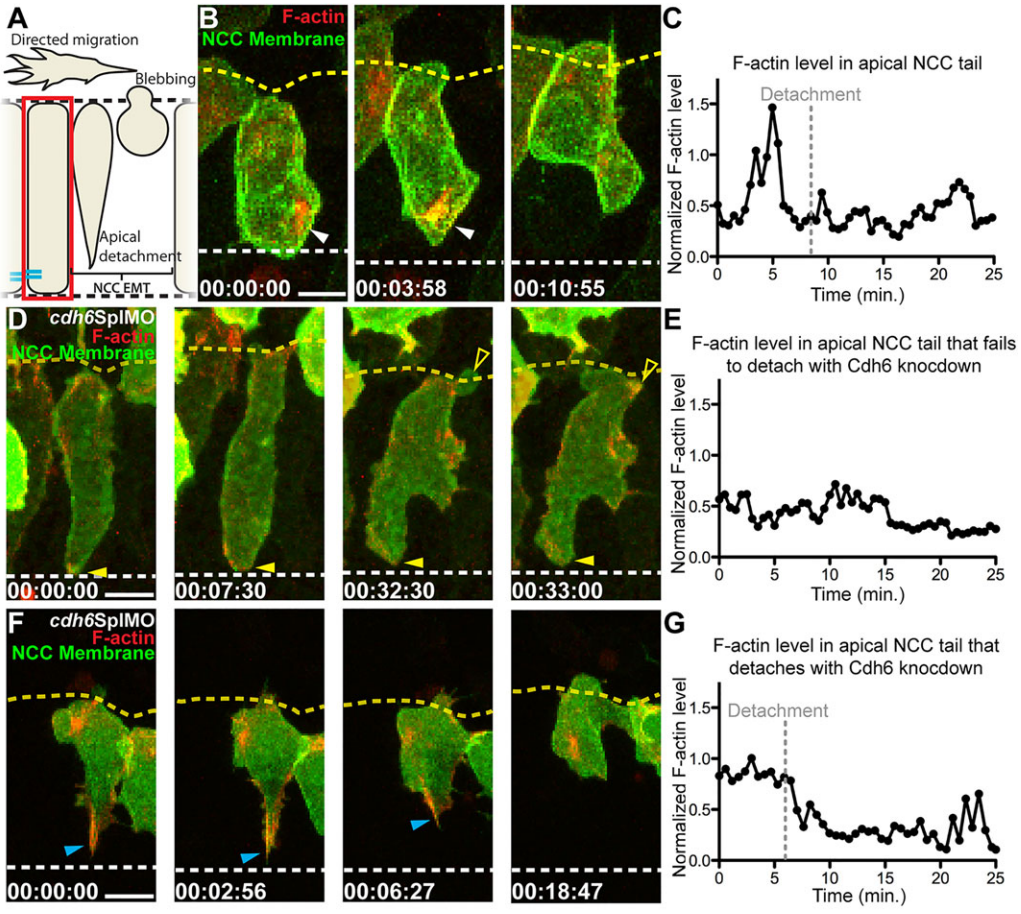

Fig. 5. Cdh6 is important for apical F-actin accumulation during NCC detachment. (A) Overview of imaging region. (B,D,F) Time-lapse images (dorsal views, anterior left, confocal z-projections beginning at 14 hpf) of NCCs expressing GFP-CAAX and F-actin biosensor (red). Yellow dashed lines mark basal neuroepithelial surfaces and white dashed lines mark apical midlines. (C,E,G) Plots of normalized F-actin intensity in apical tail over time. (B) In a control embryo, apical detachment is preceded by F-actin accumulation (white arrowheads). (C) Intensity of apical tail F-actin peaks prior to detachment in wild-type NCC shown in B. (D) After Cdh6 knockdown, F-actin does not accumulate in the apical tail (closed yellow arrowheads), the tail does not detach and the NCC does not undergo EMT. (E) Intensity of apical F-actin remains low in the Cdh6-knockdown NCC shown in B. (F) In a Cdh6-knockdown NCC that does detach and undergo EMT, F-actin accumulates apically before detachment (blue arrowheads). (G) Intensity of apical F-actin peaks before detachment in the Cdh6-knockdown NCC shown in F. Time=h:min:s. Scale bars: 10 μm.

Development (2014) 141, 2506-2515 doi:10.1242/dev.105551

Table 2. F-actin accumulation lifetimes in apical NCC tails

Group	Number of NCCs analyzed (number of embryos)	Number of NCCs in which F-actin accumulated ≤0.5 min	Number of NCCs in which F-actin accumulated >0.5 min	*P*-value (Fisher's exact test; compared with wild-type)
Wild type	6 (3)	0	6	n/a
Cdh6 knockdown (NCC fails to detach)	8 (3)	5	3	0.031
Cdh6 knockdown (NCC does detach)	2 (2)	0	2	n/a

rare NCCs that underwent EMT in Cdh6-knockdown embryos, stable F-actin did accumulate in apical tails prior to detachment (Fig. 5F,G, blue arrowheads; Table 2). Interestingly, in NCCs that failed to stabilize apical F-actin, we observed F-actin in retracting blebs, similar to what we previously found in wild-type embryos (Fig. 5D, open yellow arrowheads) (Berndt et al., 2008). These data show that Cdh6 is necessary for accumulation of apical F-actin during detachment of NCC tails, and suggest that proper regulation of this F-actin subpopulation is crucial to NCC EMT.

Cdh6 influences localization of active Rho

Rho GTPases are major regulators of cell motility and actomyosin contractile forces (Jaffe and Hall, 2005). We previously showed Rho is activated specifically in apical NCC tails before and during detachment, and that apically focused Rho activation is crucial for detachment and EMT (Clay and Halloran, 2013). Thus, we sought to determine whether Cdh6 affects Rho activation during EMT. We imaged active Rho using a biosensor containing the Rho-binding domain of Rhotekin (rGBD) fused to GFP (GFPrGBD; Benink and Bement, 2005), which we had used previously in NCCs (Clay and Halloran, 2013). We mosaically expressed the active Rho biosensor together with mCherry as a volume marker for ratiometric imaging, knocked down Cdh6 and live imaged the NCCs. We found that, similar to wild-type embryos, Rho was activated in apical NCC tails after Cdh6 knockdown (Fig. 6B,C; supplementary material Movies 5,6), although it was activated in a broader area (see below). We measured active Rho levels normalized to the basal side of the cell (R-value, see Material and Methods) and found that Rho activation significantly increased at a distinct point in time (Fig. 6D,E), similar to the increase that occurs during NCC detachment in wild-type embryos (Clay and Halloran, 2013). In Cdh6-knockdown embryos the average active Rho level before the increase (R-value=1.48) was similar to the level we reported (Clay and Halloran, 2013) for wild-type NCCs before detachment (R-value=1.36; P=0.4442, unpaired t-test). Furthermore, the average active Rho level in Cdh6 knockdown embryos after the increase (R-value=1.89) was similar to the level in wild-type embryos during EMT (R-value=1.62, P=0.0974, unpaired t-test). Therefore, loss of Cdh6 did not affect the overall level and timing of Rho activation. However, Cdh6 knockdown did influence the area of Rho activation and led to an expansion of the active Rho domain beyond the region nearest the midline (Fig. 6C, boxes). We measured the proportion of cell area occupied by active Rho and found a significant increase in Cdh6 knockdown NCCs

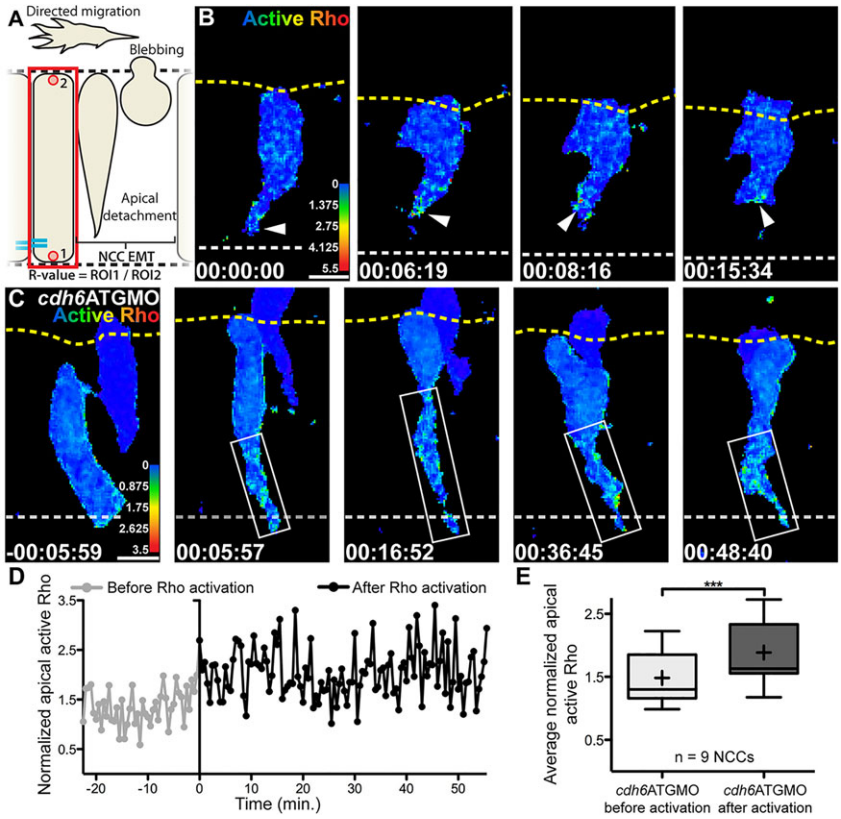

Fig. 6. Cdh6 knockdown expands area of Rho activation. (A) Overview of imaging region and definition of normalized active Rho measure (R-value). (B,C) Time-lapse images (dorsal views, anterior left, confocal z-projections beginning at 14 hpf) of NCCs expressing active Rho biosensor. Yellow dashed lines mark basal neuroepithelial surfaces and white dashed lines mark apical midlines. (B) In a control embryo, active Rho is observed primarily near the midline during NCC tail detachment (arrowheads). (C) In a Cdh6-knockdown embryo, Rho is activated but area of activation is expanded (boxes). (D) Active Rho level (R-value) over time in tail of NCC shown in C. Time when Rho activation is observed is 0 min in C,D. (E) Average active Rho level (n=9 NCCs) becomes elevated in Cdh6-knockdown embryos (***P=0.0009, paired two tailed t-test). Line is median,+is mean, box covers upper and lower quartiles, and bars encompass minimum and maximum values. Time=h:min:s. Scale bars: 10 μm.

Development (2014) 141, 2506-2515 doi:10.1242/dev.105551

(23.5% of total cell area) compared with wild-type NCCs at early detachment stages (7.9%; P=0.0017, unpaired t-test) (Clay and Halloran, 2013). These data suggest that Cdh6 may function in a novel manner to influence active Rho localization, although it may do so indirectly or in concert with other molecules (see Discussion).

DISCUSSION

Here we reveal novel functions for Cdh6 in the crucial process of EMT *in vivo*. We show that Cdh6 promotes apical detachment of hindbrain premigratory NCCs, an important early step in EMT. Moreover, we show that Cdh6 is required for the apical F-actin accumulation that precedes detachment, and for focused Rho activation, both of which are key molecular steps in EMT. These results provide new insight into signaling pathways through which Cdh6 acts, and show that Cdh6 directs localized subcellular actomyosin forces.

Our finding that Cdh6 promotes EMT is consistent with studies showing that Cdh6-mediated bone morphogenetic protein signaling promotes de-epithelialization prior to EMT in chick trunk NCCs (Park and Gumbiner, 2012, 2010). In contrast, Cdh6-mediated adhesion is thought to prevent EMT in midbrain NCCs (Coles et al., 2007). Collectively, these studies suggest diverse molecular functions for Cdh6 that may differ between trunk and cranial NCCs, and also between subpopulations of cranial NCCs (midbrain versus hindbrain). Interestingly, distinct pre-migratory cell populations within the cranial neural fold give rise to different NCC derivatives (Lee et al., 2013), and differences in cadherin expression may define subpopulations. At different stages of NCC EMT, we see little or no *cdh6* expression in the zebrafish midbrain and low levels in the hindbrain, which could indicate different roles for Cdh6 in these areas. We also see *cdh6* in neuroepithelial cells that do not undergo EMT, suggesting that Cdh6 alone is not sufficient to induce EMT and that other NCC-specific factors are likely to be involved. Interestingly, the transcription factor Snail2, a crucial driver of NCC EMT, suppresses *cdh6* expression in chick NCCs (Taneyhill et al., 2007). It is plausible that rather than completely eliminating *cdh6* expression, Snail2 maintains lower *cdh6* levels that may be crucial for EMT. Indeed, during EMT, *snail2* is expressed throughout the zebrafish neuroepithelium (Thisse et al., 1995) and hindbrain *cdh6* levels are low. After EMT, *snail2* is absent from the neuroepithelium, and *cdh6* is expressed at higher levels that may serve a different function, such as adhesion. Our finding that endogenous Cdh6 precludes expression of exogenous Cdh6-mCherry in NCC membranes further suggests that NCCs have mechanisms to tightly regulate cell-surface Cdh6 protein levels. Furthermore, our experiment showing that Cdh6 overexpression may induce early EMT suggests the timing of expression changes is crucial. Future experiments using inducible gene expression (Gerety et al., 2013) could allow for exploration of the timing of EMT relative to induction of Cdh6 expression.

An individual cadherin with multiple and sometimes opposing roles in EMT is not unprecedented. For example, Ncad adhesion suppresses NCC EMT (Nakagawa and Takeichi, 1995; Park and Gumbiner, 2010; Shoval et al., 2007), whereas its cleavage activates intracellular signals that promote EMT (Shoval et al., 2007). Ncad upregulation is thought to promote EMT in several non-neuroepithelial cells (reviewed by Wheelock et al., 2008), but in many cases Ncad expression in epithelial cells does not correlate with EMT (Dady et al., 2012; Knudsen et al., 2005; Maeda et al., 2005; Straub et al., 2011). Interestingly, it has been shown that Cdh6 also undergoes proteolytic cleavage during EMT (Schiffmacher et al., 2014), which may be one of the post-translational mechanisms by which Cdh6 is regulated during EMT. It will be interesting to see whether Cdh6 cleavage fragments also carry signaling abilities similar to Ncad or to other type II cadherins (Cad7 and Cad11), the signaling functions of which promote NCC migration (Kashef et al., 2009; McCusker et al., 2009; Nakagawa and Takeichi, 1998; Vallin et al., 1998). Overall, the end result of expressing a specific cadherin probably depends heavily on cellular context, which highlights the importance of understanding all the functions of specific cadherins during EMT *in vivo*.

We previously found that actomyosin contraction, which is promoted by Rho/ROCK signaling, is required for the detachment of NCCs but not for the accumulation of F-actin in apical NCC tails (Clay and Halloran, 2013). Here, we show that Cdh6 is necessary for apical F-actin accumulation. Interestingly, Cdh6 knockdown did not affect F-actin in NCC blebs, suggesting that Cdh6 regulates F-actin specifically in apical NCC tails. Cadherins, through adapters such as catenins, link the F-actin cytoskeleton to the cell membrane. This link may be the basis by which Cdh6 localizes F-actin apically and by which actomyosin force is transmitted into cell movement. Cdh6 has been shown to stimulate NCC de-epithelialization via non-canonical BMP signaling and LIMK-mediated inactivation of cofilin (Park and Gumbiner, 2012). The outcome of cofilin activity depends on several factors (Andrianantoandro and Pollard, 2006; Dedova et al., 2004; Pavlov et al., 2007), but active cofilin primarily functions to sever F-actin, thus disrupting F-actin networks. Furthermore, cofilin can prevent myosin II binding to F-actin, and depletion of cofilin can lead to formation of actomyosin complexes that drive contractility (Wiggan et al., 2012). As we have identified a specific subpopulation of F-actin regulated by Cdh6, we can propose a model for how Cdh6 and LIMK/cofilin act to control F-actin in NCCs (Fig. 7). A major function for Cdh6 may be to reduce cofilin activity, thereby promoting stable actomyosin which drives apical detachment. However, which molecular players control the polymerization of the F-actin seen in apical tails remains unknown. Actin nucleators, such as formins, may lead to the formation of F-actin in apical regions, which is intriguing as

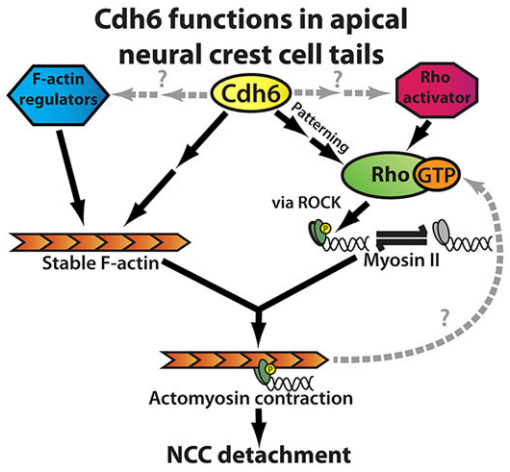

Fig. 7. Model of Cdh6 functions during EMT in apical NCC tail. Cdh6 promotes NCC detachment by promoting stable F-actin accumulation in apical tails (left). Effects of Cdh6 on F-actin may be via F-actin regulators (gray dashed arrows). Cdh6 influences active Rho localization (right) and Rho promotes actomyosin contraction during apical detachment. Cdh6 may pattern Rho activation by influencing a Rho activator and/or a feedback loop in which actomyosin affects Rho activation (dashed gray arrows). Head-to-end arrows indicate potential indirect interactions.

Development (2014) 141, 2506-2515 doi:10.1242/dev.105551

many formins are regulated by Rho GTPases (Goode and Eck, 2007). Alternatively, existing F-actin may be rearranged in a Cdh6-dependent manner to form F-actin accumulations during EMT. Either way, we have identified Cdh6 as a crucial player in the organization of F-actin during NCC EMT.

To generate the actomyosin necessary for detachment, F-actin must be coupled with myosin contractility. Rho GTPase is a key regulator of myosin (Jaffe and Hall, 2005), and the timing and location of Rho activation is determined by regulators that switch Rho on or off (Rossman et al., 2005; Tcherkezian and Lamarche-Vane, 2007). We previously showed that restriction of Rho activation to apical regions by Arhgap1 is crucial for EMT (Clay and Halloran, 2013). The expansion of Rho activation after Cdh6 knockdown suggests that Cdh6 somehow influences the Rho activation area. Cadherins have been linked to global changes in GTPase activation levels (Johnson et al., 2004; Kim et al., 2000; Kouklis et al., 2003; Kovacs et al., 2002; Lampugnani et al., 2002; Noren et al., 2003), but have not previously been implicated in influencing active GTPase localization in particular subcellular regions. Our results and model (Fig. 7) do not distinguish between direct versus indirect effects of Cdh6 on active Rho localization, and molecular steps are likely to exist between Cdh6 and Rho. One possibility is that Cdh6 knockdown causes an expansion of the apical cell domain, thus affecting localization of other apical molecules that influence Rho activity. For example, Cdh6 may influence the localization of a Rho activator within the apical cell region via an unknown mechanism, and when Cdh6 is lost the activator diffuses more broadly. It is also possible that local Rho activation is affected by actomyosin formation, and that in an attempt to overcome the detachment defect caused by loss of Cdh6 and apical F-actin, Rho is activated more broadly by Cdh6-independent molecules. These models are not mutually exclusive, and further study of direct or indirect relationships between Cdh6 and known modulators of Rho may uncover new mechanisms by which Rho regulators are localized to influence GTPase signaling. Nonetheless, it is apparent that the pathways that govern F-actin and the formation of contractile actomyosin, such as those influenced by Cdh6 and Rho, must all be coordinated for proper NCC EMT to occur.

MATERIALS AND METHODS

Animals

Animal work was carried out in compliance with guidelines from NIH and the University of Wisconsin Institutional Animal Care and Use Committee. Embryos were obtained from zebrafish wild-type lines (AB or Tuebigen), a transgenic line expressing GFP in NCCs [*Tg(-4.9sox10:EGFP)*]; Wada et al., 2005) or *ncad*^{tm101} mutants (Lele et al., 2002), and were raised at 23-28°C and staged in hpf as described previously (Kimmel et al., 1995).

DNA constructs, mRNA synthesis, morpholinos and microinjection

Full-length zebrafish *cdh6* cDNA (ZFIN; Acc: ZDB-GENE-050320-92) was amplified by RT-PCR from total RNA from 24 hpf embryos and cloned into pCS2 for *in situ* probe generation using Gateway (Life Technologies) cloning (Kwan et al., 2007).

DNA plasmids encoding C-terminal fluorescent Cdh6 fusion proteins were generated using InFusion cloning (Clontech). Full-length *cdh6* with no stop was PCR amplified from cDNA with primers that allowed InFusion reactions into target vectors. *cdh6-mCherry* was cloned into pCS2 and mMessage Machine (Life Technologies) was used to synthesize 5′-capped *cdh6-mCherry* mRNA for injections. *cdh6-GFP* was cloned behind the NCC-specific *sox10* promoter (*−4.9sox10*; Wada et al., 2005) in a vector containing *tol2* transposase sites and used for DNA injections.

All mRNA and DNA injections were carried out at the one-cell stage in a volume of 1 nl. To express Cdh6-mCherry, 125 pg of *cdh6-mCherry* mRNA was injected into embryos that express GFP in NCCs [*Tg*(*-4.9sox10:EGFP*)] allowing identification of NCCs. Injection of mRNA results in broad expression throughout the embryo. To express Cdh6-GFP specifically in NCCs, 12.5 pg of *−4.9sox10:cdh6-GFP* plasmid was injected. Injection of plasmid DNA results in mosaic expression in a subset of NCCs. Plasmids encoding membrane GFP (GFP-CAAX), mCherry, an F-actin biosensor (mCherry-UtrCH; Burkel et al., 2007), and an active Rho biosensor (GFPrGBD; Benink and Bement, 2005) driven by the *sox10* promoter were prepared as previously described (Clay and Halloran, 2013); 12.5 pg of each plasmid was injected.

Antisense morpholinos (Gene Tools) were injected into one-cell stage embryos to knock down Cdh6. A splice-blocking morpholino (*cdh6*SplMO: 5′-AGCTTTTCAAATCTTACCAATGTGA-3′) was used at 500-650 µM or a translation-blocking morpholino (*cdh6*ATGMO: 5′-AAGAAGTACAA-TCCAAGTCCTCATC-3′; Kubota et al., 2007) was used at 500 µM. To knock down Ncad, a translation-blocking morpholino (*ncad*ATGMO: 5′-TCTGTATAAAGAAACCGATAGAGTT-3′) (Lele et al., 2002) was used at 500 µM. A standard scrambled morpholino (*control*MO: 5′-CCT-CTTACCTCAGTTACAATTTATA-3′) was used as a control.

In situ hybridization

Digoxygenin-UTP- or fluorescein-labeled riboprobes for *cdh6* or *sox10* were synthesized by *in vitro* transcription and hydrolyzed to a length of ∼300 bases by limited alkaline hydrolysis (Cox et al., 1984). Whole-mount *in situ* hybridization was performed as described previously (Halloran et al., 1999). Images of colorimetric *in situ* hybridizations were acquired on a Nikon TE3000 microscope with a 20× objective using MetaMorph software (Molecular Devices). For fluorescent *in situ* hybridization, transcripts were detected by tyramide signal amplification as described previously (Lauter et al., 2011), and images were acquired on a Nikon FV1000 laser scanning confocal microscope using a 60× oil immersion objective (NA 1.35).

Western blot

Embryos were injected with *control*MO, *cdh6*SplMO or *cdh6*ATGMO and raised to 24 hpf. Protein extraction and western blotting were performed with standard techniques. To generate an antibody to zebrafish Cdh6, a peptide corresponding to Cdh6 extracellular domain amino acids 347-363 (CKNTHPYSHYMSQDTKDK) was synthesized and injected into rabbits (YenZyme Antibodies). Blots were incubated with anti-Cdh6 primary antibody at 1:500 and HRP-conjugated anti-rabbit IgG secondary antibody (115-035-174; Jackson ImmunoResearch) at 1:10,000. As a loading control, blots were incubated with anti-γ-tubulin primary antibody (T5326; Sigma-Aldrich) at 1:1000 and HRP-conjugated anti-mouse IgG secondary antibody (211-052-171; Jackson ImmunoResearch) at 1:10,000. Blots were visualized by chemiluminescence.

Cell transplantations

Cell transplantations were carried out at the blastula stage as described previously (Kemp et al., 2009). Donor embryos [*Tg(-4.9sox10:EGFP)*] were injected with 1 nl of 3% Texas Red-conjugated Dextran (Life Technologies) at the one-cell stage. Host embryos (AB) were injected with *cdh6*SplMO. At 3 hpf, cells were transplanted from donor into host embryos. Embryos were raised to 14 hpf and imaged as described below.

Live confocal imaging and analysis

For live imaging, embryos were mounted in 1% low-melting agarose in E3 with 10 mM HEPES as described previously (Andersen et al., 2010). Imaging was conducted on an Olympus FV1000 confocal microscope using a 60× oil immersion objective (NA 1.35) and began at 14 hpf. Images of hindbrain rhombomeres 1-4 were acquired every 30-35 s.

To measure Cdh6-GFP localization, maximum-intensity *z*-projections were generated. The average Cdh6-GFP intensity was auto-thresholded and measured in equal-sized regions of interest (ROIs) containing approximately one-third of the cell nearest the midline (apical) and near the lateral neuroepithelium (basal) with ImageJ. Across all cells, the mean intensities of apical and basal ROIs were compared using an unpaired one-tailed *t*-test.

For movies of GFP-CAAX-labeled NCCs, the proportion of NCCs undergoing EMT was calculated as described previously (Clay and

Development (2014) 141, 2506-2515 doi:10.1242/dev.105551

Halloran, 2013). NCCs were considered premigratory if they were in contact with both the apical midline and the basal edge of the neuroepithelium, as identified from differential interference contrast (DIC) images. EMT was considered complete when NCCs completely delaminated from the neuroepithelium. Comparisons between control and Cdh6 morpholino-injected embryos were made using Fisher's exact tests.

Embryos expressing GFP-CAAX and the mCherry-UtrCH F-actin biosensor were imaged as previously described (Clay and Halloran, 2013). To quantify the level of F-actin in the apical tail, we created a normalized fluorescence intensity measure by comparing it with the F-actin signal in blebs, which is unaffected by Cdh6 knockdown. The average mCherry intensity in a retracting bleb was measured in a 5×5 pixel ROI and averaged across three blebs in the cell. The average intensity within an ROI in the apical tail for each NCC was then normalized to the bleb intensity. To quantify the lifetime of apical F-actin accumulation, we set a threshold of normalized mCherry intensity at 0.70 (70% of the mean bleb intensity) and calculated the longest timespan above threshold for each cell. The distributions of F-actin lifetimes between wild-type and Cdh6-knockdown embryos were compared using Fisher's exact test.

The active Rho biosensor was co-expressed with mCherry as a volume marker for ratiometric imaging as previously described (Clay and Halloran, 2013). *Z*-stacks were merged and a ratio channel of GFP/mCherry fluorescence was created using Volocity software (Perkin-Elmer). The level of apical active Rho was determined by a normalized measure (R-value), which was calculated by dividing the GFP/mCherry ratio in the NCC tail by that in the leading edge. In embryos injected with Cdh6 morpholino, the R-value was averaged across all cells in two time periods: (1) during the first 20 min of imaging; and (2) during a 20 min period after Rho activation was observed. Comparison of the average R-value between periods was carried out with a paired two-tailed *t*-test. Comparisons of the average R-value from the early period in Cdh6 morpholino-injected embryos versus a similar early period in wild-type embryos, and of the average R-value following Rho activation in Cdh6 morpholino-injected embryos versus a similar period during EMT in wild-type embryos, were made using unpaired two-tailed *t*-tests.

The proportion of cell area in which Rho was activated was measured as previously described (Clay and Halloran, 2013). A threshold of active Rho was calculated from the average maximum GFP/mCherry ratio in a 20 min period. The proportion of the cell area with GFP/mCherry greater than one-third the average maximum was averaged over time. In Cdh6 morpholino-injected embryos, this period began after Rho activation was observed, and was compared with a 20 min period during wild-type EMT, when NCCs have a similar morphology, with an unpaired two-tailed *t*-test.

Statistical analysis

All statistics were calculated with Prism 5.0 (GraphPad Software). For box plots: line is median,+ is mean, box covers upper and lower quartiles, and bars encompass minimum and maximum values.

Acknowledgements

We are grateful to Bill Bement for supplying the Rho and F-actin biosensors. We thank Danielle Grotjahn and Jenya Grinblat for reagents and technical advice on the fluorescent *in situ* hybridization protocol. We thank Kevin Grunewald for technical assistance, and Bill Davis and Andrew Goelz for fish care.

Competing interests

The authors declare no competing financial interests.

Author contributions

M.R.C. and M.C.H. designed the experiments. M.R.C. performed the experiments, carried out data analysis and prepared figures. M.R.C. and M.C.H. wrote and edited the manuscript.

Funding

This work was supported by National Institutes of Health (NIH) grants [R21NS073114 to M.C.H.; R01NS042228 to M.C.H.; and F31DE022232 to M.R.C.]. The confocal microscope was acquired with an NIH shared instrumentation grant [S10RR023717]. Deposited in PMC for release after 12 months.

Supplementary material

Supplementary material available online at
http://dev.biologists.org/lookup/suppl/doi:10.1242/dev.105551/-/DC1

References

Ahlstrom, J. D. and Erickson, C. A. (2009). The neural crest epithelial-mesenchymal transition in 4D: a 'tail of multiple non-obligatory cellular mechanisms. *Development* **136**, 1801-1812.

Andersen, E., Asuri, N., Clay, M. and Halloran, M. (2010). Live imaging of cell motility and actin cytoskeleton of individual neurons and neural crest cells in zebrafish embryos. *J. Vis. Exp.* **36**, 1726.

Andrianantoandro, E. and Pollard, T. D. (2006). Mechanism of actin filament turnover by severing and nucleation at different concentrations of ADF/cofilin. *Mol. Cell* **24**, 13-23.

Benink, H. A. and Bement, W. M. (2005). Concentric zones of active RhoA and Cdc42 around single cell wounds. *J. Cell Biol.* **168**, 429-439.

Bergert, M., Chandradoss, S. D., Desai, R. A. and Paluch, E. (2012). Cell mechanics control rapid transitions between blebs and lamellipodia during migration. *Proc. Natl. Acad. Sci. U.S.A.* **109**, 14434-14439.

Berndt, J. D., Clay, M. R., Langenberg, T. and Halloran, M. C. (2008). Rho-kinase and myosin II affect dynamic neural crest cell behaviors during epithelial to mesenchymal transition in vivo. *Dev. Biol.* **324**, 236-244.

Betson, M., Lozano, E., Zhang, J. and Braga, V. M. M. (2002). Rac activation upon cell-cell contact formation is dependent on signaling from the epidermal growth factor receptor. *J. Biol. Chem.* **277**, 36962-36969.

Bravo-Cordero, J. J., Sharma, V. P., Roh-Johnson, M., Chen, X., Eddy, R., Condeelis, J. and Hodgson, L. (2013). Spatial regulation of RhoC activity defines protrusion formation in migrating cells. *J. Cell Sci.* **126**, 3356-3369.

Bryant, D. M., Wylie, F. G. and Stow, J. L. (2005). Regulation of endocytosis, nuclear translocation, and signaling of fibroblast growth factor receptor 1 by E-cadherin. *Mol. Biol. Cell* **16**, 14-23.

Burkel, B. M., von Dassow, G. and Bement, W. M. (2007). Versatile fluorescent probes for actin filaments based on the actin-binding domain of Utrophin. *Cell Motil. Cytoskeleton* **64**, 822-832.

Charrasse, S., Meriane, M., Comunale, F., Blangy, A. and Gauthier-Rouvière, C. (2002). N-cadherin-dependent cell-cell contact regulates Rho GTPases and beta-catenin localization in mouse C2C12 myoblasts. *J. Cell Biol.* **158**, 953-965.

Charrasse, S., Comunale, F., Fortier, M., Portales-Casamar, E., Debant, A. and Gauthier-Rouvière, C. (2007). M-cadherin activates Rac1 GTPase through the Rho-GEF trio during myoblast fusion. *Mol. Biol. Cell* **18**, 1734-1743.

Clay, M. R. and Halloran, M. C. (2013). Rho activation is apically restricted by Arhgap1 in neural crest cells and drives epithelial-to-mesenchymal transition. *Development* **140**, 3198-3209.

Coles, E. G., Taneyhill, L. A. and Bronner-Fraser, M. (2007). A critical role for Cadherin6B in regulating avian neural crest emigration. *Dev. Biol.* **312**, 533-544.

Cox, K. H., DeLeon, D. V., Angerer, L. M. and Angerer, R. C. (1984). Detection of mRNAs in sea urchin embryos by in situ hybridization using asymmetric RNA probes. *Dev. Biol.* **101**, 485-502.

Dady, A., Blavet, C. and Duband, J.-L. (2012). Timing and kinetics of E- to N-cadherin switch during neurulation in the avian embryo. *Dev. Dyn.* **241**, 1333-1349.

Dedova, I. V., Nikolaeva, O. P., Mikhailova, V. V., dos Remedios, C. G. and Levitsky, D. I. (2004). Two opposite effects of cofilin on the thermal unfolding of F-actin: a differential scanning calorimetric study. *Biophys. Chem.* **110**, 119-128.

Doherty, P., Williams, G. and Williams, E.-J. (2000). CAMs and axonal growth: a critical evaluation of the role of calcium and the MAPK cascade. *Mol. Cell. Neurosci.* **16**, 283-295.

Gerety, S. S., Breau, M. A., Sasai, N., Xu, Q., Briscoe, J. and Wilkinson, D. G. (2013). An inducible transgene expression system for zebrafish and chick. *Development* **140**, 2235-2243.

Goode, B. L. and Eck, M. J. (2007). Mechanism and function of formins in the control of actin assembly. *Annu. Rev. Biochem.* **76**, 593-627.

Halloran, M. C., Severance, S. M., Yee, C. S., Gemza, D. L., Raper, J. A. and Kuwada, J. Y. (1999). Analysis of a zebrafish semaphorin reveals potential functions in vivo. *Dev. Dyn.* **214**, 13-25.

Hatta, K., Takagi, S., Fujisawa, H. and Takeichi, M. (1987). Spatial and temporal expression pattern of N-cadherin cell adhesion molecules correlated with morphogenetic processes of chicken embryos. *Dev. Biol.* **120**, 215-227.

Heasman, S. J., Carlin, L. M., Cox, S., Ng, T. and Ridley, A. J. (2010). Coordinated RhoA signaling at the leading edge and uropod is required for T cell transendothelial migration. *J. Cell Biol.* **190**, 553-563.

Inoue, T., Chisaka, O., Matsunami, H. and Takeichi, M. (1997). Cadherin-6 expression transiently delineates specific rhombomeres, other neural tube subdivisions, and neural crest subpopulations in mouse embryos. *Dev. Biol.* **183**, 183-194.

Itoh, R. E., Kurokawa, K., Ohba, Y., Yoshizaki, H., Mochizuki, N. and Matsuda, M. (2002). Activation of rac and cdc42 video imaged by fluorescent resonance energy transfer-based single-molecule probes in the membrane of living cells. *Mol. Cell. Biol.* **22**, 6582-6591.

Jaffe, A. B. and Hall, A. (2005). Rho GTPases: biochemistry and biology. *Annu. Rev. Cell Dev. Biol.* **21**, 247-269.
Johnson, E., Theisen, C. S., Johnson, K. R. and Wheelock, M. J. (2004). R-cadherin influences cell motility via Rho family GTPases. *J. Biol. Chem.* **279**, 31041-31049.
Kashef, J., Koehler, A., Kuriyama, S., Alfandari, D., Mayor, R. and Wedlich, D. (2009). Cadherin-11 regulates protrusive activity in Xenopus cranial neural crest cells upstream of Trio and the small GTPases. *Genes Dev.* **23**, 1393-1398.
Kemp, H. A., Carmany-Rampey, A. and Moens, C. (2009). Generating chimeric zebrafish embryos by transplantation. *J. Vis. Exp.* **1394**.
Kim, S. H., Li, Z. and Sacks, D. B. (2000). E-cadherin-mediated cell-cell attachment activates Cdc42. *J. Biol. Chem.* **275**, 36999-37005.
Kimmel, C. B., Ballard, W. W., Kimmel, S. R., Ullmann, B. and Schilling, T. F. (1995). Stages of embryonic development of the zebrafish. *Dev. Dyn.* **203**, 253-310.
Knudsen, K. A., Sauer, C., Johnson, K. R. and Wheelock, M. J. (2005). Effect of N-cadherin misexpression by the mammary epithelium in mice. *J. Cell. Biochem.* **95**, 1093-1107.
Kouklis, P., Konstantoulaki, M. and Malik, A. B. (2003). VE-cadherin-induced Cdc42 signaling regulates formation of membrane protrusions in endothelial cells. *J. Biol. Chem.* **278**, 16230-16236.
Kovacs, E. M., Ali, R. G., McCormack, A. J. and Yap, A. S. (2002). E-cadherin homophilic ligation directly signals through Rac and phosphatidylinositol 3-kinase to regulate adhesive contacts. *J. Biol. Chem.* **277**, 6708-6718.
Kubota, F., Murakami, T., Mogi, K. and Yorifuji, H. (2007). Cadherin-6 is required for zebrafish nephrogenesis during early development. *Int. J. Dev. Biol.* **51**, 123-129.
Kwan, K. M., Fujimoto, E., Grabher, C., Mangum, B. D., Hardy, M. E., Campbell, D. S., Parant, J. M., Yost, H. J., Kanki, J. P. and Chien, C.-B. (2007). The Tol2kit: a multisite Gateway-based construction kit for Tol2 transposon transgenesis constructs. *Dev. Dyn.* **236**, 3088-3099.
Lampugnani, M. G., Zanetti, A., Breviario, F., Balconi, G., Orsenigo, F., Corada, M., Spagnuolo, R., Betson, M., Braga, V. and Dejana, E. (2002). VE-cadherin regulates endothelial actin activating Rac and increasing membrane association of Tiam. *Mol. Biol. Cell* **13**, 1175-1189.
Lauter, G., Söll, I. and Hauptmann, G. (2011). Multicolor fluorescent in situ hybridization to define abutting and overlapping gene expression in the embryonic zebrafish brain. *Neural Dev.* **6**, 10.
Lee, R. T. H., Nagai, H., Nakaya, Y., Sheng, G., Trainor, P. A., Weston, J. A. and Thiery, J. P. (2013). Cell delamination in the mesencephalic neural fold and its implication for the origin of ectomesenchyme. *Development* **140**, 4890-4902.
Lele, Z., Folchert, A., Concha, M., Rauch, G.-J., Geisler, R., Rosa, F., Wilson, S. W., Hammerschmidt, M. and Bally-Cuif, L. (2002). parachute/n-cadherin is required for morphogenesis and maintained integrity of the zebrafish neural tube. *Development* **129**, 3281-3294.
Liu, Q., Liu, B., Wilson, A. L. and Rostedt, J. (2006). *cadherin-6* message expression in the nervous system of developing zebrafish. *Dev. Dyn.* **235**, 272-278.
Machacek, M., Hodgson, L., Welch, C., Elliott, H., Pertz, O., Nalbant, P., Abell, A., Johnson, G. L., Hahn, K. M. and Danuser, G. (2009). Coordination of Rho GTPase activities during cell protrusion. *Nature* **461**, 99-103.
Maeda, M., Johnson, K. R. and Wheelock, M. J. (2005). Cadherin switching: essential for behavioral but not morphological changes during an epithelium-to-mesenchyme transition. *J. Cell Sci.* **118**, 873-887.
Matthews, H. K., Marchant, L., Carmona-Fontaine, C., Kuriyama, S., Larrain, J., Holt, M. R., Parsons, M. and Mayor, R. (2008). Directional migration of neural crest cells in vivo is regulated by Syndecan-4/Rac1 and non-canonical Wnt signaling/RhoA. *Development* **135**, 1771-1780.
McCusker, C., Cousin, H., Neuner, R. and Alfandari, D. (2009). Extracellular cleavage of cadherin-11 by ADAM metalloproteases is essential for Xenopus cranial neural crest cell migration. *Mol. Biol. Cell* **20**, 78-89.
Nakagawa, S. and Takeichi, M. (1995). Neural crest cell-cell adhesion controlled by sequential and subpopulation-specific expression of novel cadherins. *Development* **121**, 1321-1332.
Nakagawa, S. and Takeichi, M. (1998). Neural crest emigration from the neural tube depends on regulated cadherin expression. *Development* **125**, 2963-2971.
Nakaya, Y., Sukowati, E. W., Wu, Y. and Sheng, G. (2008). RhoA and microtubule dynamics control cell-basement membrane interaction in EMT during gastrulation. *Nat. Cell. Biol.* **10**, 765-775.
Nalbant, P., Hodgson, L., Kraynov, V., Toutchkine, A. and Hahn, K. M. (2004). Activation of endogenous Cdc42 visualized in living cells. *Science* **305**, 1615-1619.
Nieman, M. T., Prudoff, R. S., Johnson, K. R. and Wheelock, M. J. (1999). N-cadherin promotes motility in human breast cancer cells regardless of their E-cadherin expression. *J. Cell Biol.* **147**, 631-644.
Nieto, A. (2011). The ins and outs of the epithelial to mesenchymal transition in health and disease. *Annu. Rev. Cell Dev. Biol.* 27, 347-376.
Noren, N. K., Arthur, W. T. and Burridge, K. (2003). Cadherin engagement inhibits RhoA via p190RhoGAP. *J. Biol. Chem.* **278**, 13615-13618.
Park, K.-S. and Gumbiner, B. M. (2010). Cadherin 6B induces BMP signaling and de-epithelialization during the epithelial mesenchymal transition of the neural crest. *Development* **137**, 2691-2701.
Park, K.-S. and Gumbiner, B. M. (2012). Cadherin-6B stimulates an epithelial mesenchymal transition and the delamination of cells from the neural ectoderm via LIMK/cofilin mediated non-canonical BMP receptor signaling. *Dev. Biol.* **366**, 232-243.
Pavlov, D., Muhlrad, A., Cooper, J., Wear, M. and Reisler, E. (2007). Actin filament severing by cofilin. *J. Mol. Biol.* **365**, 1350-1358.
Perrais, M., Chen, X., Perez-Moreno, M. and Gumbiner, B. M. (2007). E-cadherin homophilic ligation inhibits cell growth and epidermal growth factor receptor signaling independently of other cell interactions. *Mol. Biol. Cell* **18**, 2013-2025.
Pertz, O., Hodgson, L., Klemke, R. L. and Hahn, K. M. (2006). Spatiotemporal dynamics of RhoA activity in migrating cells. *Nature* **440**, 1069-1072.
Provenzano, P. P. and Keely, P. J. (2011). Mechanical signaling through the cytoskeleton regulates cell proliferation by coordinated focal adhesion and Rho GTPase signaling. *J. Cell Sci.* **124**, 1195-1205.
Qian, X., Karpova, T., Sheppard, A. M., McNally, J. and Lowy, D. R. (2004). E-cadherin-mediated adhesion inhibits ligand-dependent activation of diverse receptor tyrosine kinases. *EMBO J.* **23**, 1739-1748.
Rossman, K. L., Der, C. J. and Sondek, J. (2005). GEF means go: turning on Rho GTPases with guanine nucleotide-exchange factors. *Nat. Rev. Mol. Cell Biol.* **6**, 167-180.
Sahai, E. and Marshall, C. J. (2003). Differing modes of tumour cell invasion have distinct requirements for Rho/ROCK signalling and extracellular proteolysis. *Nat. Cell. Biol.* **5**, 711-719.
Schiffmacher, A. T., Padmanabhan, R., Jhingory, S. and Taneyhill, L. A. (2014). Cadherin-6B is proteolytically processed during epithelial-to-mesenchymal transitions of the cranial neural crest. *Mol. Biol. Cell* **25**, 41-54.
Shoval, I., Ludwig, A. and Kalcheim, C. (2007). Antagonistic roles of full-length N-cadherin and its soluble BMP cleavage product in neural crest delamination. *Development* **134**, 491-501.
Skaper, S. D., Moore, S. E. and Walsh, F. S. (2001). Cell signalling cascades regulating neuronal growth-promoting and inhibitory cues. *Prog. Neurobiol.* **65**, 593-608.
Straub, B. K., Rickelt, S., Zimbelmann, R., Grund, C., Kuhn, C., Iken, M., Ott, M., Schirmacher, P. and Franke, W. W. (2011). E-N-cadherin heterodimers define novel adherens junctions connecting endoderm-derived cells. *J. Cell Biol.* **195**, 873-887.
Taneyhill, L. A., Coles, E. G. and Bronner-Fraser, M. (2007). Snail2 directly represses cadherin6B during epithelial-to-mesenchymal transitions of the neural crest. *Development* **134**, 1481-1490.
Taniuchi, K., Nakagawa, H., Hosokawa, M., Nakamura, T., Eguchi, H., Ohigashi, H., Ishikawa, O., Katagiri, T. and Nakamura, Y. (2005). Overexpressed P-cadherin/CDH3 promotes motility of pancreatic cancer cells by interacting with p120ctn and activating rho-family GTPases. *Cancer Res.* **65**, 3092-3099.
Tcherkezian, J. and Lamarche-Vane, N. (2007). Current knowledge of the large RhoGAP family of proteins. *Biol. Cell* **99**, 67-86.
Thiery, J. P., Acloque, H., Huang, R. Y. J. and Nieto, M. A. (2009). Epithelial-mesenchymal transitions in development and disease. *Cell* **139**, 871-890.
Thisse, C., Thisse, B. and Postlethwait, J. H. (1995). Expression of *snail2*, a second member of the zebrafish snail family, in cephalic mesendoderm and presumptive neural crest of wild-type and *spadetail* mutant embryos. *Dev. Biol.* **172**, 86-99.
Tozluoğlu, M., Tournier, A. L., Jenkins, R. P., Hooper, S., Bates, P. A. and Sahai, E. (2013). Matrix geometry determines optimal cancer cell migration strategy and modulates response to interventions. *Nat. Cell. Biol.* **15**, 751-762.
Vallin, J., Girault, J.-M., Thiery, J. P. and Broders, F. (1998). Xenopus cadherin-11 is expressed in different populations of migrating neural crest cells. *Mech. Dev.* **75**, 171-174.
Wada, N., Javidan, Y., Nelson, S., Carney, T. J., Kelsh, R. N. and Schilling, T. F. (2005). Hedgehog signaling is required for cranial neural crest morphogenesis and chondrogenesis at the midline in the zebrafish skull. *Development* **132**, 3977-3988.
Wheelock, M. J., Shintani, Y., Maeda, M., Fukumoto, Y. and Johnson, K. R. (2008). Cadherin switching. *J. Cell Sci.* **121**, 727-735.
Wiggan, O., Shaw, A. E., DeLuca, J. G. and Bamburg, J. R. (2012). ADF/cofilin regulates actomyosin assembly through competitive inhibition of myosin II binding to F-actin. *Dev. Cell* **22**, 530-543.